Sheffield Hallam University

Thermoelectric performance of Na-doped GeSe

SHAABANI, Laaya, AMINORROAYA YAMINI, Sima <http://orcid.org/0000-0002-2312-8272>, BYRNES, Jacob, AKBAR NEZHAD, Ali and BLAKE, Graeme

Available from Sheffield Hallam University Research Archive (SHURA) at:

http://shura.shu.ac.uk/18189/

This document is the author deposited version. You are advised to consult the publisher's version if you wish to cite from it.

Published version

Repository use policy

Sheffield Hallam University Research Archive
http://shura.shu.ac.uk

ACS OMEGA

Thermoelectric Performance of Na-Doped GeSe

Laaya Shaabani,[†] Sima Aminorroaya-Yamini,*[‡,§] Jacob Byrnes,[‡] Ali Akbar Nezhad,[||] and Graeme R. Blake*[†]

[†]Zernike Institute for Advanced Materials, University of Groningen, Nijenborgh 4, Groningen 9747AG, The Netherlands
[‡]Australian Institute for Innovative Materials, Innovation Campus, University of Wollongong, Wollongong, NSW 2500, Australia
[§]Department of Engineering and Mathematics, Sheffield Hallam University, Sheffield S11WB, U.K.
[||]School of Civil and Environmental Engineering, University of New South Wales, Sydney, NSW 2052, Australia

ABSTRACT: Recently, hole-doped GeSe materials have been predicted to exhibit extraordinary thermoelectric performance owing largely to extremely low thermal conductivity. However, experimental research on the thermoelectric properties of GeSe has received less attention. Here, we have synthesized polycrystalline Na-doped GeSe compounds, characterized their crystal structure, and measured their thermoelectric properties. The Seebeck coefficient decreases with increasing Na content up to $x = 0.01$ due to an increase in the hole carrier concentration and remains roughly constant at higher concentrations of Na, consistent with the electrical resistivity variation. However, the electrical resistivity is large for all samples, leading to low power factors. Powder X-ray diffraction and scanning electron microscopy/energy-dispersive spectrometry results show the presence of a ternary impurity phase within the GeSe matrix for all doped samples, which suggests that the optimal carrier concentration cannot be reached by doping with Na. Nevertheless, the lattice thermal conductivity and carrier mobility of GeSe is similar to those of polycrystalline samples of the leading thermoelectric material SnSe, leading to quality factors of comparable magnitude. This implies that GeSe shows promise as a thermoelectric material if a more suitable dopant can be found.
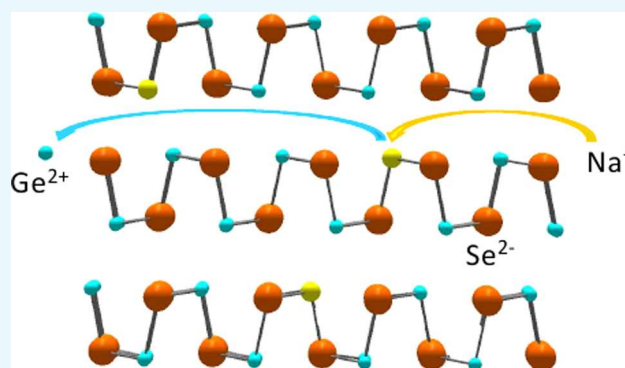
INTRODUCTION

Thermoelectric (TE) materials have been intensively investigated over the past decades due to their ability to convert waste heat to electricity, especially in view of the energy crisis and concern for the environment.[1−3] The performance of a TE material is determined by its dimensionless figure of merit (zT), defined as $zT = (S^2\sigma T)/\kappa$, where S is the Seebeck coefficient, σ is the electrical conductivity, κ is the total thermal conductivity, and T is the absolute temperature.[4−6] There is an ongoing search for new materials with high TE efficiency, especially using environmentally friendly and abundant elements, as well as the development of several approaches to improve the zT of existing materials via optimizing the parameters S, σ, and κ.[4,7−10] Chalcogenide compounds have been extensively studied and their TE performance has shown significant enhancement in recent years.[11,12] High thermoelectric performance has recently been reported for single crystals of SnSe, largely due to their ultralow thermal conductivity.[13] High zT values and low thermal conductivities are also reported in polycrystalline SnSe, but their power factor values are significantly lower than those of single crystals.[14−23] Germanium telluride (GeTe)-based materials have also been widely studied for their promising thermoelectric properties.[24−29] However, germanium selenide (GeSe) has received little attention for thermoelectric applications despite its use in

other applications, such as optoelectronics,[30,31] resistive memory cells,[32] glass-forming materials for photonic devices with thin-film structures,[33,34] photovoltaic applications,[30] and resistive switching materials.[32,35]

GeSe is a p-type narrow-band gap semiconductor ($E_g = 1.1-1.2$ eV)[36,37] that adopts a layered orthorhombic crystal structure at room temperature with space group *Pnma*, isostructural with GeS, SnS, and SnSe.[38] Only a few reports have been published on the transport properties of GeSe; these mostly focus on the electrical conductivity[36,37,39−43] with only two reports on the thermal conductivity of GeSe.[44,45] Recently, a theoretical study predicted the thermoelectric performance of orthorhombic IV−VI compounds GeS, SnSe, SnS, and GeSe using density functional theory combined with the Boltzmann transport theory.[46] It is proposed that GeS, SnS, and GeSe show thermoelectric properties comparable to those of SnSe, which makes them promising candidates for high-efficiency thermoelectric applications.[46] Another modeling study using similar methods predicted extremely high thermoelectric performance in hole-doped GeSe crystals along the *b*-crystallographic direction, with a figure of merit ranging from
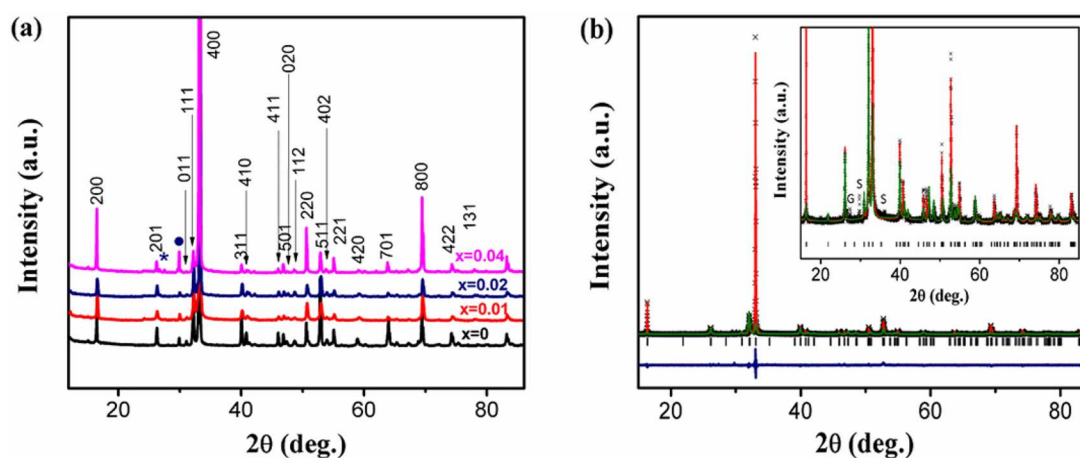
Figure 1. (a) Room temperature XRD patterns of the powder $Ge_{1−x}Na_xSe$ (x = 0.00, 0.01, 0.02, and 0.04) samples. The star indicates a graphite peak originating from the carbon-coated quartz tube, and the circle at ∼30° indicates a peak from the sample holder. (b) Observed (black data points), fitted (red line), and difference (blue line) XRD profiles for the x = 0.02 sample. The fit used the March−Dollase preferred orientation model incorporated in the GSAS software. The green line represents the best fit obtained without any preferred orientation model. The inset shows a closer view of the fits; the symbols G and S indicate graphite and sample holder peaks, respectively.

0.8 at 300 K to 2.5 at 800 K. This represents an even higher calculated figure of merit than that of hole-doped SnSe, which holds the current experimental record for high zT among bulk systems.[47] Thus, it is highly desired to experimentally explore the thermoelectric performance of GeSe-based materials. A recent study[45] reports a maximum zT of 0.16 at 700 K for Ag-doped polycrystalline $Ge_{0.79}Ag_{0.01}Sn_{0.2}Se$ by achieving carrier concentrations of ∼10^{18} cm$^{−3}$. Better TE performance is predicted at higher carrier concentrations, which was impossible to obtain by silver doping.

In this study, we have fabricated polycrystalline pristine and Na-doped GeSe samples and measured their thermoelectric properties. We have found that the lattice thermal conductivity of our samples is significantly higher than the ultralow values predicted theoretically[47] but at <0.8 W m$^{−1}$ K$^{−1}$ above 550 K for the pristine sample is in good agreement with the previous experimental report in ref 45. Doping with 1 and 2% Na reduces κ to <0.7 and ∼0.5 W m$^{−1}$ K$^{−1}$, respectively, in the same temperature range. However, the power factors of the Na-doped samples are low due to the formation of Na-rich precipitates, which prevents optimal carrier concentrations from being reached. Nevertheless, the measured carrier mobility of GeSe is comparable with that of SnSe; thus, GeSe may be a promising thermoelectric material if a more suitable dopant is identified.

METHODS

Synthesis. Polycrystalline $Ge_{1−x}Na_xSe$ samples with x = 0.00, 0.01, 0.02, and 0.04 were synthesized using a melting technique. Stoichiometric ratios of high-purity elements, Ge (99.999%, Alfa Aesar), Se (99.999%, Alfa Aesar), and Na (99%, Aldrich), were weighed in an argon atmosphere glovebox with a total mass of 10 g and loaded into carbon-coated quartz tubes. The tubes were sealed under vacuum, slowly heated to 1223 K, and held at that temperature for 10 h. The samples were then quenched in cold water, followed by annealing at 673 K for 72 h. The ingots obtained were hand-ground into fine powder using an agate mortar and pestle and loaded into a 12 mm diameter graphite die. The powders were then sintered using spark plasma sintering at 623 K for 30 min under an axial pressure of 40 MPa in vacuum.

X-ray Diffraction (XRD). X-ray diffraction measurements were performed using a GBC Scientific X-ray diffractometer with Cu Kα radiation (λ = 1.5406 Å, 40 kV, 25 mA) at room temperature. The structural parameters were extracted from the X-ray diffraction patterns by the Rietveld refinement method using the GSAS software suite.[48]

Electron Microscopy Analysis. The microstructures of the samples were studied using a high-resolution scanning electron microscope (SEM), JEOL JSM-7001, equipped with an energy-dispersive X-ray spectrometer (EDS).

Transport Properties Measurements. The Hall coefficient (R_H) was measured by an in-house-built apparatus using the van der Pauw technique (perpendicular to the hot-pressing direction) in vacuum under magnetic fields of up to ±1.5 T. The Hall carrier concentration, n, was obtained using $n = (1/e) R_H$, where e is the elementary charge and R_H is the Hall coefficient. Disc-shaped pellets with densities ∼94% of the theoretical density, 12 mm diameter, and 2 mm thickness were used for this measurement. The electrical conductivity (σ) and Seebeck coefficient (S) were measured simultaneously under 0.1 atm helium from room temperature to 573 K using a Linseis LSR-3 instrument. The samples for measurement were cut from pressed pellets and polished into a parallelepiped shape; measurements were performed in the in-plane direction. The thermal diffusivity, D, was measured by the laser flash diffusivity method (Linseis LFA 1000) in the out-of-plane direction over the temperature range 300−573 K. The specific heat capacity (C_p) was calculated using the equation C_p (GeSe, (298.15−940) K) = ((46.777 + 15.099) × 10$^{−3}T$ − 0.0316 × 10$^{−6}T^2$ − 1.231 × 10^5 $T^{−2}$) J K$^{−1}$ mol$^{−1}$.[49] The thermal conductivity (κ) was calculated using $\kappa = \rho D C_p$, where the density (ρ) of the pellets was calculated by measuring the mass and dimensions.

RESULTS AND DISCUSSION

Figure 1 shows the room temperature powder X-ray diffraction (XRD) patterns of the $Ge_{1−x}Na_xSe$ compounds (x = 0.00, 0.01, 0.02, and 0.04). The main peaks of all samples could be indexed on the basis of the orthorhombic α-GeSe structure, with the unit cell parameters a = 10.8419(9) Å, b = 3.8389(6) Å, and c = 4.3951(7) Å (space group, $Pnma$). Each primitive unit cell of α-
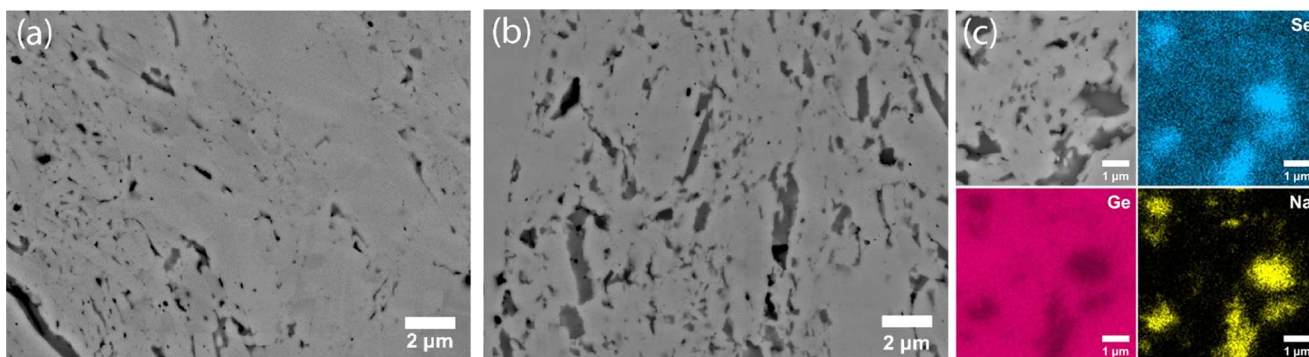
Figure 2. BSE images of (a) $Ge_{0.99}Na_{0.01}Se$ and (b) $Ge_{0.96}Na_{0.04}Se$. A secondary phase (darker gray) is observed in the GeSe matrix (lighter gray). (c) EDS characterization: BSE images of $Ge_{0.96}Na_{0.04}Se$ showing a secondary phase within the GeSe matrix, with EDS elemental mapping for Ge, Se, and Na. The secondary phase appears to be higher in Na and Se concentration and lower in Ge concentration than the surrounding GeSe matrix.
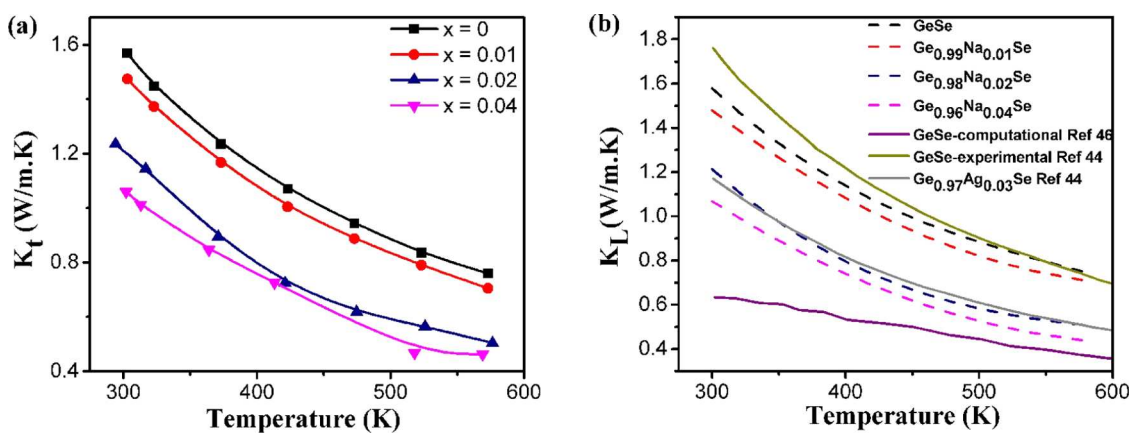
Figure 3. (a) Measured total thermal conductivity, κ_t, of $Ge_{1-x}Na_xSe$ (x = 0.00, 0.01, 0.02, and 0.04) in the temperature range 300−573 K. (b) Calculated lattice thermal conductivity, κ_L, of $Ge_{1-x}Na_xSe$ (x = 0.00, 0.01, 0.02, and 0.04) compared with theoretical values[47] calculated along the *b*-axis and experimental values from ref 45.

GeSe phase consists of eight atoms, which form two zigzag double layers. Each atom is coordinated to three nearest neighbors within its own layer and three more distant neighbors in adjacent layers; there is weak van der Waals bonding between adjacent layers and strong covalent interactions within the layers.[39,50,51] This phase is reported to transform to the high-symmetry cubic rocksalt structure ($Fm\overline{3}m$, β-GeSe) at a temperature of 853 K (a = 5.73 Å).[52−54] The unit cell parameters do not change (within error bars) on doping. X-ray diffraction analysis was performed on powders and pellets. For powder samples there is strong preferred orientation along the [100] direction (that is, the layer stacking direction in the crystallites tends to be perpendicular to the sample surface), which makes the 400 peak very strong. A similar degree of preferred orientation was observed in the X-ray diffraction patterns of the pellets, as shown in Figure 1b. This implies that the thermal conductivity was measured more along the *a*-direction, whereas the electrical resistivity and Seebeck coefficient measurements were performed largely in the *bc*-plane. Microstructural analysis of lightly and heavily doped GeSe samples was conducted by scanning electron microscopy (SEM). Figure 2a,b shows representative back-scattered electron (BSE) images of $Ge_{0.99}Na_{0.01}Se$ and $Ge_{0.96}Na_{0.04}Se$, respectively. Precipitates are distributed in the GeSe matrix for both samples. The precipitates appear to vary in size and concentration with respect to the Na concentration. Precipitates of <1 μm are most

common in $Ge_{0.99}Na_{0.01}Se$, whereas those observed in $Ge_{0.96}Na_{0.04}Se$ are typically 1−5 μm in size. The concentration of precipitates also appears to be increased for $Ge_{0.96}Na_{0.04}Se$.

To probe the chemical composition of the secondary phase, energy-dispersive X-ray spectroscopy (EDS) mapping was used. Figure 2c shows the EDS elemental map of precipitates within the GeSe matrix for the $Ge_{0.96}Na_{0.04}Se$ sample. The precipitates are richer in Na and Se and poorer in Ge than the matrix, suggesting that sodium doping induces the formation of a ternary sodium germanium selenide as a secondary phase. The concentration of precipitates is too low to give rise to extra peaks in the XRD patterns; thus, the phase could not be identified.

Figure 3a shows the total thermal conductivity, κ_t, of the $Ge_{1-x}Na_xSe$ (x = 0.00, 0.01, 0.02, and 0.04) compounds as a function of temperature in the range of 300−573 K. The thermal conductivity for all samples decreases with temperature. The thermal conductivity of the undoped sample is 1.57 W m^{-1} K^{-1} at 300 K, which is reduced to 0.76 W m^{-1} K^{-1} at 573 K. This is significantly lower than the previously measured values in polycrystalline samples of 2.2 and 1.3 W m^{-1} K^{-1} at 300 and 573 K, respectively, in ref 44 but comparable to the values of 1.8 and 0.8 W m^{-1} K^{-1} reported in ref 45 at the same temperatures. We note that the Dulong−Petit approximation of the specific heat capacity was used for GeSe in ref 45; if used for our samples, the thermal conductivity plotted in Figure 3a would be ~10% lower at 573 K. Figure 3a also shows that the

total thermal conductivity decreases with increasing dopant concentration and that samples with precipitates possess much lower thermal conductivity than lightly doped samples. The lattice thermal conductivity (Figure 3b) was obtained by subtracting the electronic contribution, κ_e, from the measured total thermal conductivity $\kappa_L = \kappa_t - \kappa_e$. The value of κ_e can be estimated via the Wiedemann–Franz law, $\kappa_e = L\sigma T$, where σ is the electrical conductivity and L is the Lorenz number, which was calculated by using a single parabolic band model with the acoustic phonon scattering assumption.[55] These estimated lattice thermal conductivities are compared with the previously predicted[47] and measured[45] values in Figure 3b. The results indicate that the lattice thermal conductivity is the predominant part of the total thermal conductivity in agreement with the low carrier concentration of $\sim 2 \times 10^{16}$ cm^{-3} obtained by Hall effect measurement for the pristine sample at room temperature and indicating that the electronic contribution to the total thermal conductivity is negligible ($\sim 10^{-6} - 10^{-5}$ W m^{-1} K^{-1}). However, the lattice thermal conductivity of the undoped sample is higher than the extraordinarily low values of ~ 0.6 and 0.4 W m^{-1} K^{-1} predicted for GeSe along the b-axis[47] at 300 and 573 K, respectively. The lattice thermal conductivity is reduced with Na content up to $x = 0.04$, for which we measure $\kappa_L = 0.44$ W m^{-1} K^{-1} at 573 K. This originates from the scattering of phonons at an increased density of interfaces and defects due to the distribution of precipitates within the matrix.[56,57] Such a decrease in κ_L has also been observed for Ag-doped GeSe,[45] although the possible presence of precipitates was not investigated in that study. Similarly, the alloying of 5% GeSe and 5% GeS with GeTe led to a reduction in κ_L by almost 50% compared to that of pristine GeTe; although large precipitates of several microns in size were observed, the reduction in κ_L was attributed mostly to point defects and mass fluctuations.[58]

In the calculations of thermal conductivity in ref 47, charge carrier concentrations of $(4-6.5) \times 10^{19}$ cm^{-3} were used because this range is predicted to yield optimal zT. The electronic component of the thermal conductivity κ_e remains small for this range of carrier concentration, of the order of 0.2 W m^{-1} K^{-1} at 600 K; thus, the calculations predict that the total thermal conductivity of GeSe should be even lower than that of SnSe. This would result in an extremely high predicted figure of merit of 2.1 at 600 K.[47] However, our results suggest that the predicted values for thermal conductivity[47] are underestimated unless the optimal carrier concentration can be reached while also maintaining a distribution of precipitates.

Table 1 compares the room temperature transport properties of Na-doped polycrystalline GeSe in our study compared to those of Na-doped polycrystalline GeSe in another recent experimental report[45] in which pellets with preferred orientation comparable to our samples were measured using the same geometry. The thermal conductivities of the low-

doped samples are very similar, but our study yields lower thermal conductivity for heavily doped samples. The electrical resistivity of our samples is much lower than the reported values in ref 45 for samples with the same composition ($Ge_{0.98}Na_{0.02}Se$ and $Ge_{0.96}Na_{0.04}Se$).

The electrical resistivity of the $Ge_{1-x}Na_xSe$ samples with $x = 0.00, 0.01, 0.02$, and 0.04 is shown as a function of temperature in the range 300–580 K in Figure 4a. The electrical resistivity decreases monotonically with temperature for all samples and remains roughly constant at temperatures above 450 K. At room temperature, sodium doping reduces the electrical resistivity of GeSe significantly from 1.0×10^6 mΩ cm for the undoped sample to 7.9×10^4 mΩ cm for $x = 0.01$, roughly by a factor of 12. However, further doping beyond $x = 0.01$ has no beneficial effect; the electrical resistivity of the $x = 0.02$ and 0.04 samples is slightly higher, probably because the doping limit is soon reached and additional sodium is incorporated into the precipitate phase. The Seebeck coefficients (S) of all samples as a function of the temperature are shown in Figure 4b. The positive values over the entire temperature range indicate that all samples are p-type semiconductors. The Seebeck coefficients increase with temperature over the whole temperature range except for the undoped sample that exhibits a maximum value at ~ 450 K. The so-called bipolar effect, the increasing contribution of minority carriers to the transport properties with temperature due to thermal excitation across the band gap,[59] is commonly observed in narrow-band gap materials. Although our samples show no sign of a bipolar effect over the temperature range in which measurements were performed (300–580 K), we note that a bipolar effect was observed at temperatures above 600 K in a previous work on GeSe.[45] Because the band gap of GeSe is relatively wide (~ 1.1 eV[36,37]), at temperatures below 600 K, the probability of thermal excitation of the electrons to the conduction band is low, which results in suppression of the bipolar effect in this range of temperatures. Undoped GeSe shows the largest Seebeck coefficient ($S = 990$ μV K^{-1}) at 450 K. The Seebeck coefficient is smallest throughout the studied temperature range for the $x = 0.01$ sample, whereas the $x = 0.02$ and 0.04 samples exhibit similar and slightly larger values, which is consistent with the variation of the electrical resistivity because both the Seebeck coefficient and electrical resistivity are inversely proportional to the carrier concentration. This indicates that the carrier concentration increases with dopant concentration up to $x = 0.01$, beyond which it remains roughly constant. This result is in agreement with the SEM analysis where the concentration of precipitates is shown to increase with dopant concentration (Figure 2).

It was first proposed by Chasmar and Stratton[60] that to achieve a higher figure of merit in a thermoelectric semi-conducting compound, a material parameter known as the thermoelectric quality factor, B, must be improved. The quality factor can be used to evaluate the performance of a thermoelectric material through the combination of several fundamental parameters.[60-65]

$$B = \left(\frac{k_B}{e}\right)^2 \frac{2e(k_B T)^{3/2}}{(2\pi)^{3/2}\hbar^3} \frac{N_V \mu_0 m_b^{*3/2}}{\kappa_L} T$$

Here, k_B is the Boltzmann constant, $\hbar$ is the reduced Planck constant, N_V is the band degeneracy, m_b^* is the density of states effective mass of a single band, μ_0 is the mobility at the nondegenerate limit, T is the temperature, and κ_L is the lattice

Table 1. Transport Properties of GeSe Doped with Na at 300 K

composition	S (μV K^{-1})	ρ (mΩ cm)	κ_t (W m^{-1} K^{-1})
$Ge_{0.98}Na_{0.02}Se$[45]	627	6.81×10^5	1.48
$Ge_{0.96}Na_{0.04}Se$[45]	631	2.99×10^7	1.40
$Ge_{0.94}Na_{0.06}Se$[45]	501	3.39×10^7	1.43
$Ge_{0.99}Na_{0.01}Se$ (our work)	471	0.79×10^5	1.47
$Ge_{0.98}Na_{0.02}Se$ (our work)	508	1.71×10^5	1.23
$Ge_{0.96}Na_{0.04}Se$ (our work)	505	1.84×10^5	1.06
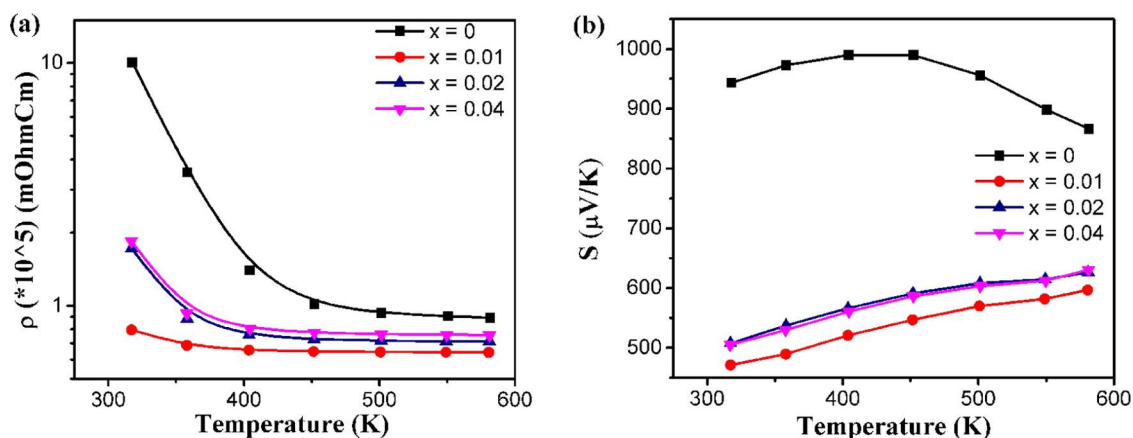
Figure 4. (a) Logarithmic temperature dependence of the electrical resistivity of $Ge_{1-x}Na_xSe$ (x = 0.00, 0.01, 0.02, and 0.04) in the temperature range 300−580 K. (b) Temperature dependence of the Seebeck coefficient of $Ge_{1-x}Na_xSe$ (x = 0.00, 0.01, 0.02, and 0.04) in the temperature range 300−580 K.

Table 2. Parameters that Determine Quality Factor B for SnSe and GeSe

parameters	T (K)	κ_L (W m^{-1} K^{-1})	μ_0 (cm^2 V^{-1} s^{-1})	B
SnSe (n-type)	580	0.5−0.75[14,15,66]	20[15 a]	$(28.54−42.81) \times 10^{45} \times m_b^{*3/2}$
GeSe	580	0.76	34.75	$48.94 \times 10^{45} \times m_b^{*3/2}$

^{a}Value measured at 750 K; μ_0 = 45 cm^2 V^{-1} s^{-1} at 300 K.

thermal conductivity. The potential of doped GeSe compounds as good thermoelectric materials can be evaluated by comparing the quality factor of undoped GeSe with that of SnSe, assuming similar band structures. Table 2 shows the quality factors estimated for polycrystalline GeSe and SnSe at 580 K and the parameters used (or ranges of parameters in cases where a quantity has been reported in more than one study). Here, we assume that the measured values of mobility correspond to μ_0 at the nondegenerate limit, which has been shown for SnSe to be a valid approximation.[15] Taking into account the large uncertainty in these parameters, which are likely to be very sensitive to sample quality and small variations in stoichiometry, the two materials have similar quality factors. Therefore, it is likely that the thermoelectric performance of GeSe can be improved by choosing an effective dopant and by consequent band structure engineering.

CONCLUSIONS

In summary, we have investigated the effect of Na doping on the thermoelectric performance of GeSe. We have synthesized $Ge_{1-x}Na_xSe$ (x = 0−0.04) compounds and measured their thermoelectric properties. Our experimental results show that the substitution of Na for Ge in GeSe gives rise to the formation of Na-rich precipitates within the GeSe matrix and thus that Na is an unsuitable dopant for GeSe. Although the power factor of these samples is low because the optimal carrier concentration cannot be reached, GeSe could nevertheless be a promising thermoelectric material if suitably doped because it shows intrinsically low lattice thermal conductivity. The presence of Na-rich precipitates decreases the lattice thermal conductivity by around 50% to ∼0.5 W m^{-1} K^{-1} at 500 K; thus, a codoping strategy may be a fruitful approach to optimizing the thermoelectric performance of GeSe. Furthermore, the carrier mobility of GeSe is similar to that of the leading thermoelectric material SnSe, giving a similar thermoelectric quality factor. Therefore, identifying an effective dopant might

lead to significant improvement in the thermoelectric figure of merit in GeSe-based materials.

AUTHOR INFORMATION

Corresponding Authors

*E-mail: s.aminorroaya@shu.ac.uk (S.A.-Y.).
*E-mail: g.r.blake@rug.nl (G.R.B.).

ORCID

Sima Aminorroaya-Yamini: 0000-0002-2312-8272
Graeme R. Blake: 0000-0001-9531-7649

Notes

The authors declare no competing financial interest.

REFERENCES

(1) Snyder, G. J.; Toberer, E. S. Complex Thermoelectric Materials. *Nat. Mater.* **2008**, *7*, 105−114.

(2) DiSalvo, F. J. Thermoelectric cooling and power generation. *Science* **1999**, *285*, 703−706.

(3) Yang, J.; Caillat, T. Thermoelectric materials for space and automotive power generation. *MRS Bull.* **2006**, *31*, 224−229.

(4) Goldsmid, H. J. Conversion Efficiency and Figure-of-Merit. In *CRC Handbook of Thermoelectrics*; Rowe, D. M., Ed.; CRC Press: Boca Raton, 1995; pp 19−26.

(5) Heremans, J. P.; Dresselhaus, M. S.; Bell, L. E.; Morelli, D. T. When thermoelectrics reached the nanoscale. *Nat. Nanotechnol.* **2013**, *8*, 471−473.

(6) Zhao, L. D.; Dravid, V. P.; Kanatzidis, M. G. The panoscopic approach to high performance thermoelectrics. *Energy Environ. Sci.* **2014**, *7*, 251−268.

(7) Zhang, Q.; He, J.; Zhu, T. J.; Zhang, S. N.; Zhao, X. B.; Tritt, T. M. High figures of merit and natural nanostructures in $Mg_2Si_{0.4}Sn_{0.6}$ based thermoelectric materials. *Appl. Phys. Lett.* **2008**, *93*, No. 102109.

(8) Poudel, B.; Hao, Q.; Ma, Y.; Lan, Y.; Minnich, A.; Yu, B.; Yan, X.; Wang, D.; Muto, A.; Vashaee, D.; Chen, X.; Liu, J.; Dresselhaus, M. S.; Chen, G.; Ren, Z. High-thermoelectric performance of nanostructured bismuth antimony telluride bulk alloys. *Science* **2008**, *320*, 634−638.

(9) Hochbaum, A. I.; Chen, R.; Delgado, R. D.; Liang, W.; Garnett, E. C.; Najarian, M.; Majumdar, A.; Yang, P. Enhanced thermoelectric performance of rough silicon nanowires. *Nature* **2008**, *451*, 163−167.

(10) Zebarjadi, M.; Esfarjani, K.; Dresselhaus, M. S.; Ren, A. F.; Chen, G. Perspectives on thermoelectrics: from fundamentals to device applications. *Energy Environ. Sci.* **2012**, *5*, 5147−5162.

(11) Pei, Y.; LaLonde, A. D.; Iwanaga, S.; Snyder, G. J. High thermoelectric figure of merit in heavy hole dominated PbTe. *Energy Environ Sci.* **2011**, *4*, 2085−2089.

(12) LaLonde, A. D.; Pei, Y.; Snyder, G. J. Reevaluation of $PbTe_{1−x}I_x$ as high performance n-type thermoelectric material. *Energy Environ. Sci.* **2011**, *4*, 2090−2096.

(13) Zhao, L.-D.; Lo, S.-H.; Zhang, Y.; Sun, H.; Tan, G.; Uher, C.; Wolverton, C.; Dravid, V. P.; Kanatzidis, M. G. Ultralow thermal conductivity and high thermoelectric figure of merit in SnSe crystals. *Nature* **2014**, *508*, 373−377.

(14) Sassi, S.; Candolfi, C.; Vaney, J. B.; Ohorodniichuk, V.; Masschelein, P.; Dauscher, A.; Lenoir, B. Assessment of the thermoelectric performance of polycrystalline p-type SnSe. *Appl. Phys. Lett.* **2014**, *104*, No. 212105.

(15) Chen, C.-L.; Wang, H.; Chen, Y.-Y.; Day, T.; Snyder, G. J. Thermoelectric properties of p-type polycrystalline SnSe doped with Ag. *J. Mater. Chem. A* **2014**, *2*, 11171−11176.

(16) Ding, J.; Xu, B.; Lin, Y.; Nan, C.; Liu, W. *New J. Phys.* **2015**, *17*, No. 083012.

(17) Wei, T.-R.; Wu, C.-F.; Zhang, X.; Tan, Q.; Sun, L.; Pan, Y.; Li, J.-F. Thermoelectric transport properties of pristine and Na-doped $SnSe_{1−x}Te_x$ polycrystals. *Phys. Chem. Chem. Phys.* **2015**, *17*, 30102−30109.

(18) Zhang, Q.; Chere, E. K.; Sun, J.; Cao, F.; Dahal, K.; Chen, S.; Chen, G.; Ren, Z. Studies on thermoelectric properties of n-type polycrystalline $SnSe_{1−x}S_x$ by iodine doping. *Adv. Energy Mater.* **2015**, *5*, No. 1500360.

(19) Carrete, J.; Mingo, N.; Curtarolo, S. Low thermal conductivity and triaxial phononic anisotropy of SnSe. *Appl. Phys. Lett.* **2014**, *105*, No. 101907.

(20) Banik, A.; Biswas, K. Lead-free thermoelectrics: promising thermoelectric performance in p-type $SnTe_{1−x}Se_x$ system. *J. Mater. Chem. A* **2014**, *2*, 9620−9625.

(21) Chere, E. K.; Zhang, Q.; Dahal, K.; Cao, F.; Mao, J.; Ren, Z. Studies on thermoelectric figure of merit of Na-doped p-type polycrystalline SnSe. *J. Mater. Chem. A* **2016**, *4*, 1848−1854.

(22) Han, Y.-M.; Zhao, J.; Zhou, M.; Jiang, X.-X.; Leng, H.-Q.; Li, L.-F. Thermoelectric performance of SnS and SnS-SnSe solid solution. *J. Mater. Chem. A* **2015**, *3*, 4555−4559.

(23) Ge, Z.-H.; Wei, K.; Lewis, H.; Martin, J.; Nolas, G. S. Bottom-up processing and low temperature transport properties of polycrystalline SnSe. *J. Solid State Chem.* **2015**, *225*, 354−358.

(24) Levin, E. M.; Besser, M. F.; Hanus, R. Electronic and thermal transport in GeTe: A versatile base for thermoelectric materials. *J. Appl. Phys.* **2013**, *114*, No. 083713.

(25) Lewis, J. E. The defect structure of non-stoichiometric germanium telluride from magnetic susceptibility measurements. *Phys. Status Solidi B* **1970**, *38*, 131−140.

(26) Christakudi, T. A.; Plachkova, S. K.; Christakudis, G. C. Thermoelectric power of $(GeTe)_{1−x}(Bi_2Te_3)_x$ solid solutions ($0 \leq x \leq 0.05$) in the temperature interval 80 to 350 K. *Phys. Status Solidi A* **1995**, *147*, 211−220.

(27) Damon, D. H.; Lubell, M. S.; Mazelsky, R. Nature of the defects in germanium telluride. *J. Phys. Chem. Solids* **1967**, *28*, 520−522.

(28) Perumal, S.; Roychowdhury, S.; Negi, D. S.; Datta, R.; Biswas, K. High thermoelectric performance and enhanced mechanical stability of p-type $Ge_{1−x}Sb_xTe$. *Chem. Mater.* **2015**, *27*, 7171−7178.

(29) Perumal, S.; Roychowdhury, S.; Biswas, K. High performance thermoelectric materials and devices based on GeTe. *J. Mater. Chem. C* **2016**, *4*, 7520−7536.

(30) Antunez, P. D.; Buckley, J. J.; Brutchey, R. L. Tin and germanium monochalcogenide IV−VI semiconductor nanocrystals for use in solar cells. *Nanoscale* **2011**, *3*, 2399−2411.

(31) Xiao, G.; Wang, Y.; Ning, J.; Wei, Y.; Liu, B.; Yu, W. W.; Zou, G.; Zou, B. Recent advances in IV−VI semiconductor nanocrystals: synthesis, mechanism, and applications. *RSC Adv.* **2013**, *3*, 8104−8130.

(32) Bräuhaus, D.; Schindler, C.; Bottger, U.; Waser, R. Radio-frequency sputter deposition of germanium selenide thin films for resistive switching. *Thin Solid Films* **2008**, *516*, 1223−1226.

(33) Sharma, P.; Rangra, V. S.; Sharma, P.; Katyal, S. C. Effect of antimony addition on the optical behaviour of germanium selenide thin films. *J. Phys. D: Appl. Phys.* **2008**, *41*, No. 225307.

(34) Lezal, D.; Pedlikova, J.; Zavadil, J. Chalcogenide glasses for optical and photonics applications. *J. Optoelectron. Adv. Mater.* **2004**, *6*, 133−137.

(35) Kügeler, C.; Rosezin, R.; Linn, E.; Bruchhaus, R.; Waser, R. Materials, technologies, and circuit concepts for nanocrossbar-based bipolar RRAM. *Appl. Phys. A: Mater. Sci. Process.* **2011**, *102*, 791−809.

(36) Asanabe, S.; Okazaki, A. Electrical properties of germanium selenide GeSe. *J. Phys. Soc. Jpn.* **1960**, *15*, 989−997.

(37) Vaughn, D. D., II; Sun, D.; Levin, S. M.; Biacchi, A. J.; Mayer, T. S.; Schaak, R. E. Colloidal synthesis and electrical properties of GeSe nanobelts. *Chem. Mater.* **2012**, *24*, 3643−3649.

(38) Sist, M.; Gatti, C.; Nørby, P.; Cenedese, S.; Kasai, H.; Kato, K.; Iversen, B. B. High-temperature crystal structure and chemical bonding in thermoelectric germanium selenide (GeSe). *Chem. - Eur. J.* **2017**, *23*, 6888−6895.

(39) Makinistian, L.; Albanesi, E. A. Ab initio calculations of the electronic and optical properties of germanium selenide. *J. Phys.: Condens. Matter* **2007**, *19*, No. 186211.

(40) Onodera, A.; Sakamoto, I.; Fujii, Y.; Môri, N.; Sugai, S. Structural and electrical properties of GeSe and GeTe at high pressure. *Phys. Rev. B* **1997**, *56*, 7935−7941.

(41) Mukherjee, B. Layered Chalcogenides Nanostructures: Synthesis, Characterization and Optoelectrical Applications. Ph.D. Thesis, National University of Singapore, 2013.

(42) Kyriakos, D. S.; Anagnostopoulos, A. N. Electrical conductivity of layered GeSe related to extended faults. *J. Appl. Phys.* **1985**, *58*, 3917−3920.

(43) Solanki, G. K.; Deshpande, M. P.; Agarwal, M. K.; Patel, P. D.; et al. Thermoelectric power factor measurements in GeSe single crystals grown using different transporting agents. *J. Mater. Sci. Lett.* **2003**, *22*, 985−987.

(44) Okhotin, A. S.; Krestovnikov, A. N.; Aivazov, A. A.; Pushkarskii, A. S. Thermal conductivity of GeS and GeSe. *Phys. Status Solidi B* **1969**, *31*, 485−487.

(45) Zhang, X.; Shen, J.; Lin, S.; Li, J.; Chen, Z.; Li, W.; Pei, Y. Thermoelectric properties of GeSe. *J. Materiomics* **2016**, *2*, 331−337.

(46) Ding, G.; Gao, G.; Yao, K. High-efficient thermoelectric materials: the case of orthorhombic IV-VI compounds. *Sci. Rep.* **2015**, *5*, No. 9567.

(47) Hao, S.; Shi, F.; Dravid, V. P.; Kanatzidis, M. G.; Wolverton, C. Computational prediction of high thermoelectric performance in hole doped layered GeSe. *Chem. Mater.* **2016**, *28*, 3218−3226.

(48) Tobey, B. H. EXPGUI, a graphical user interface for GSAS. *J. Appl. Crystallogr.* **2001**, *34*, 210−213.

(49) Olin, A.; Noläng, B.; Osadchii, E. G.; Öhman, L. O.; Rosén, E. *Chemical Thermodynamics of Selenium*; Elsevier: Amsterdam, 2005; Vol. 7, p 209.

(50) Taniguchi, M.; Johnson, R. L.; Ghijsen, J.; Cardona, M. Core excitons and conduction-band structures in orthorhombic GeS, GeSe, SnS, and SnSe single crystals. *Phys. Rev. B* **1990**, *42*, 3634−3643.

(51) Okazaki, A. The crystal structure of germanium selenide GeSe. *J. Phys. Soc. Jpn.* **1958**, *13*, 1151−1155.

(52) Vaughn, D. D., II; Patel, R. J.; Hickner, M. A.; Schaak, R. E. Single-crystal colloidal nanosheets of GeS and GeSe. *J. Am. Chem. Soc.* **2010**, *132*, 15170−15172.

(53) Wiedemeier, H.; Siemers, P. A. The thermal expansion and high temperature transformation of GeSe. *Z. Anorg. Allg. Chem.* **1975**, *411*, 90−96.

(54) Dutta, S. N.; Jeffrey, G. A. On the structure of germanium selenide and related binary IV/VI compounds. *Inorg. Chem.* **1965**, *4*, 1363−1366.

(55) Kim, H.-S.; Gibbs, Z. M.; Tang, Y.; Wang, H.; Snyder, G. J. Characterization of Lorenz number with Seebeck coefficient measurement. *APL Mater.* **2015**, *3*, No. 041506.

(56) Aminorroaya Yamini, S.; Mitchell, D. R. G.; Gibbs, Z. M.; Santos, R.; Patterson, V.; Li, S.; Pei, Y. Z.; Dou, S. X.; Snyder, G. J. Heterogeneous distribution of sodium for high thermoelectric performance of p-type multiphase lead-chalcogenides. *Adv. Energy Mater.* **2015**, *5*, No. 1501047.

(57) Aminorroaya Yamini, S.; Wang, H.; Gibbs, Z. M.; Pei, Y.; Mitchell, D. R. G.; Dou, S. X.; Snyder, G. J. Thermoelectric performance of tellurium-reduced quaternary p-type lead-chalcogenide composites. *Acta Mater.* **2014**, *80*, 365−372.

(58) Samanta, M.; Biswas, K. Low Thermal Conductivity and High Thermoelectric Performance in $(GeTe)_{1-2x}(GeSe)_x(GeS)_x$: Competition between Solid Solution and Phase Separation. *J. Am. Chem. Soc.* **2017**, *139*, 9382−9391.

(59) Wu, H.; Chang, C.; Feng, D.; Xiao, Y.; Zhang, X.; Pei, Y.; Zheng, L.; Wu, D.; Gong, S.; Chen, Y.; He, J.; Kanatzidis, M. G.; Zhao, L.-D. Synergistically optimized electrical and thermal transport properties of SnTe via alloying high-solubility MnTe. *Energy Environ. Sci.* **2015**, *8*, 3298−3312.

(60) Chasmar, R. P.; Stratton, R. The thermoelectric figure of merit and its relation to thermoelectric generators. *J. Electron. Control* **1959**, *7*, 52−72.

(61) Nolas, G. S.; Sharp, J.; Goldsmid, H. J. *Thermoelectrics - Basic Principles and New Materials Developments*; Springer-Verlag: Berlin, Heidelberg, 2001.

(62) Mahan, G. D. Good Thermoelectrics. In *Solid State Physics*; Ehrenreich, H., Spaepen, F., Eds.; Academic Press: San Diego, 1997; Vol. *51*, pp 81−157.

(63) Goldsmid, H. J. *Introduction to Thermoelectricity*; Springer-Verlag: Berlin, Heidelberg, 2010.

(64) Goldsmid, H. J. *Thermoelectric Refrigeration*; Temple Press Books Ltd.: London, 1964.

(65) Wang, H.; Pei, Y.; LaLonde, A. D.; Snyder, G. J. Material Design Considerations Based on Thermoelectric Quality Factor. In *Thermoelectric Nanomaterials*; Koumoto, K., Mori, T., Eds.; Springer-Verlag: Berlin, Heidelberg, 2013; pp 3−32.

(66) Fu, Y.; Xu, J.; Liu, G.-Q.; Yang, J.; Tan, X.; Liu, Z.; Qin, H.; Shao, H.; Jiang, H.; Liang, B.; Jiang, J. Enhanced thermoelectric performance in p-type polycrystalline SnSe benefiting from texture modulation. *J. Mater. Chem. C* **2016**, *4*, 1201−1207.